# Supplementary Material for Temperature-dependent mean inner potential of polystyrene spheres measured by off-axis electron holography

Yan Lu*[1], Peng-Han Lu[1], Fengshan Zheng[1,2], Dominik Biscette[3], Denys Sutter[3], Johan Chang[3], Giulio Pozzi[1,4], and Rafal E. Dunin-Borkowski[1]

[1]Ernst Ruska-Centre for Microscopy and Spectroscopy with Electrons, Forschungszentrum Jülich GmbH, 52428 Jülich, Germany
[2]Spin-X Institute, Electron Microscopy Center, School of Physics and Optoelectronics, State Key Laboratory of Luminescent Materials and Devices, Guangdong-Hong Kong-Macao Joint Laboratory of Optoelectronic and Magnetic Functional Materials, South China University of Technology, Guangzhou, China
[3]CondenZero AG, 8050 Zürich, Switzerland
[4]Department FIM, University of Modena and Reggio Emilia, via G. Campi 213/a, 41125 Modena, Italy

## 1 Phase shift contributed by MIP

Assuming a sphere with radius $R$ and its center at (0, 0, 0), it is written in Cartesian coordinates as $x^2 + y^2 + z^2 = R^2$, along $z$ axis, i.e. beam direction, the phase shift induced by MIP is in the form

$$\varphi_{\mathrm{MIP}} = C_{\mathrm{E}} \int_{-\sqrt{R^2-x^2-y^2}}^{\sqrt{R^2-x^2-y^2}} V_{\mathrm{MIP}}\, dz = 2C_{\mathrm{E}} V_{\mathrm{MIP}} \sqrt{R^2 - x^2 - y^2}. \tag{1}$$

## 2 Electrostatic phase shift inside projected sphere area

The electrostatic potential from a point charge $Q$ at (0,0,0) and its compensating charge $-Q$ at ($x_0$, $y_0$, 0) is written in the form

$$V = V_{\mathrm{Q}} + V_0 = \frac{Q}{4\pi\epsilon_0}\Big(\frac{1}{\sqrt{x^2+y^2+z^2}} - \frac{1}{\sqrt{(x-x_0)^2+(y-y_0)^2+z^2}}\Big). \tag{2}$$

The projected phase shift outside of a charged sphere can be easily derived by infinite integral of a point charge dipole, as described in Eq. (3) in the main text:

$$\varphi_{\mathrm{Q}}(x,y) = C_{\mathrm{E}} \frac{Q}{4\pi\epsilon_0} \ln \frac{(x-x_0)^2+(y-y_0)^2}{x^2+y^2}$$

As to the electrostatic potential inside the sphere, we consider two situations of homogeneous charge distribution: surface charge and volume charge.

## 2.1 Constant surface charge density

On the surface and inside the sphere, the electrostatic potential from the surface charge is

$$V_{\mathrm{S}} = \frac{Q}{4\pi\epsilon_0 R}. \tag{3}$$

The projected phase shift is contributed by $V_S$, potential above and below the sphere from $V_Q$, and potential from the image charge. It can be written in the form

$$\begin{aligned}
\varphi_{\mathrm{Q}} =& C_{\mathrm{E}}\Big( \int_{-\sqrt{R^2-x^2-y^2}}^{\sqrt{R^2-x^2-y^2}} V_{\mathrm{S}}\, dz + \int_{-\infty}^{-\sqrt{R^2-x^2-y^2}} V_{\mathrm{Q}}\, dz + \int_{\sqrt{R^2-x^2-y^2}}^{\infty} V_{\mathrm{Q}}\, dz + \int_{-\infty}^{\infty} V_0\, dz \Big) \\
=& 2C_{\mathrm{E}}\frac{Q}{4\pi\epsilon_0}\Big( \frac{\sqrt{R^2-x^2-y^2}}{R} + \int_{\sqrt{R^2-x^2-y^2}}^{\infty} \frac{1}{\sqrt{x^2+y^2+z^2}}\, dz \\
& - \int_0^{\infty} \frac{1}{\sqrt{(x-x_0)^2+(y-y_0)^2+z^2}}\, dz \Big) \\
=& 2C_{\mathrm{E}}\frac{Q}{4\pi\epsilon_0}\Big( \frac{\sqrt{R^2-x^2-y^2}}{R} + \ln(z+\sqrt{x^2+y^2+z^2})\Big|_{\sqrt{R^2-x^2-y^2}}^{\infty} \\
& - \ln(z+\sqrt{(x-x_0)^2+(y-y_0)^2+z^2})\Big|_0^{\infty} \Big) \\
=& 2C_{\mathrm{E}}\frac{Q}{4\pi\epsilon_0}\Big( \frac{\sqrt{R^2-x^2-y^2}}{R} + \ln\frac{\sqrt{(x-x_0)^2+(y-y_0)^2}}{\sqrt{R^2-x^2-y^2}+R} \Big).
\end{aligned} \tag{4}$$

The phase simulation of a 226-nm sphere with constant surface charge density is shown in Fig. S1a. The charge amount is 200 e.

## 2.2 Constant volume charge density

Inside sphere, the electrostatic potential from a uniformly volume charged sphere is [1]

$$V_{\mathrm{B}} = \frac{Q}{8\pi\epsilon_0 R^3}(3R^2 - x^2 - y^2 - z^2). \tag{5}$$

The projected potential can be written as

$$\begin{aligned}
\varphi_{\mathrm{Q}} =& C_{\mathrm{E}}\Big( \int_{-\sqrt{R^2-x^2-y^2}}^{\sqrt{R^2-x^2-y^2}} V_{\mathrm{B}}\, dz + \int_{-\infty}^{-\sqrt{R^2-x^2-y^2}} V_{\mathrm{Q}}\, dz + \int_{\sqrt{R^2-x^2-y^2}}^{\infty} V_{\mathrm{Q}}\, dz + \int_{-\infty}^{\infty} V_0\, dz \Big) \\
=& C_{\mathrm{E}}\frac{Q}{8\pi\epsilon_0 R^3}\Big[ (3R^2-x^2-y^2)z - \frac{z^3}{3} \Big]\Big|_{-\sqrt{R^2-x^2-y^2}}^{\sqrt{R^2-x^2-y^2}} \\
& + 2C_{\mathrm{E}}\frac{Q}{4\pi\epsilon_0}\Big( \int_{\sqrt{R^2-x^2-y^2}}^{\infty} \frac{1}{\sqrt{x^2+y^2+z^2}}\, dz - \int_0^{\infty} \frac{1}{\sqrt{(x-x_0)^2+(y-y_0)^2+z^2}}\, dz \Big) \\
=& 2C_{\mathrm{E}}\frac{Q}{8\pi\epsilon_0 R^3}\Big[ 2R^2\sqrt{R^2-x^2-y^2} + \frac{2}{3}(R^2-x^2-y^2)\sqrt{R^2-x^2-y^2} \Big]
\end{aligned}$$

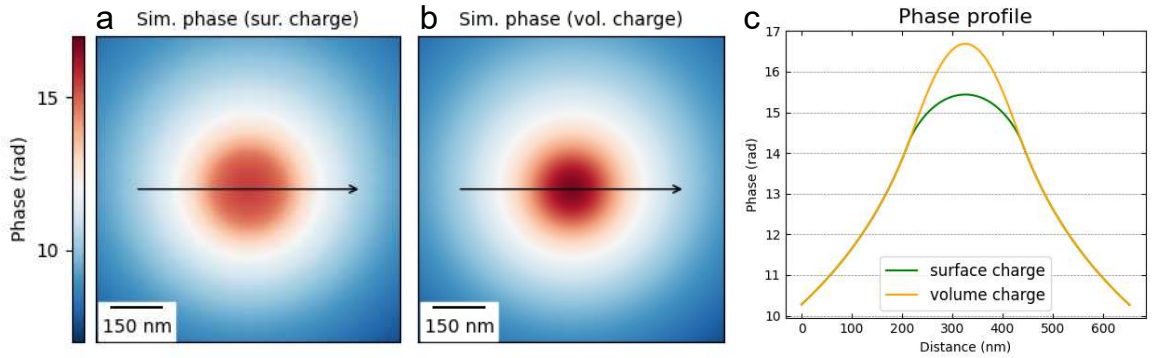


Figure S1: Simulated phase of surface-charged and volume-charge of a 226-nm sphere with charge amount of 200 e, and the phase profile from each.

$$+2C_{\mathrm{E}}\frac{Q}{4\pi\epsilon_0}\left[\ln(z+\sqrt{x^2+y^2+z^2})\Big|^{\infty}_{\sqrt{R^2-x^2-y^2}}-\ln(z+\sqrt{(x-x_0)^2+(y-y_0)^2+z^2})\Big|^{\infty}_{0}\right]$$

$$=C_{\mathrm{E}}\frac{Q}{4\pi\epsilon_0 R^3}\frac{2}{3}\sqrt{R^2-x^2-y^2}(4R^2-x^2-y^2)+2C_{\mathrm{E}}\frac{Q}{4\pi\epsilon_0}\ln\frac{\sqrt{(x-x_0)^2+(y-y_0)^2}}{\sqrt{R^2-x^2-y^2}+R}. \quad (6)$$

The phase simulation of a 226-nm sphere with constant volume charge density is shown in Fig. S1b. The charge amount is 200 e. Figure S1c shows the phase profile along the arrows.

## 2.3 Simulation vs. experiment

The simulation of a sphere with both surface charge and volume charge are shown in Fig. S2. Figure S2a show simulated phase of surface charge of of a uniformly surface-charged sphere with diameter of 226 nm, charge amount of 200 e and MIP of 5.5 V. Figure S2b displays the cumulative charge within the dashed box while the charge is distributed on surface (green line) and in volume (orange line). It is clear that the charge increases differently depending on the distribution. The details of cumulative charge will be addressed in Section 3. Figures S2c and d are the equi-phase line of spacing $2\pi/4$ of a uniformly surface-charged and volume-charged sphere, respectively. It can be seen that the difference with the previous case over the whole image is hardly detectable by eye, apart in the central region. A better evaluation is provided by the line scans, as done in the following.

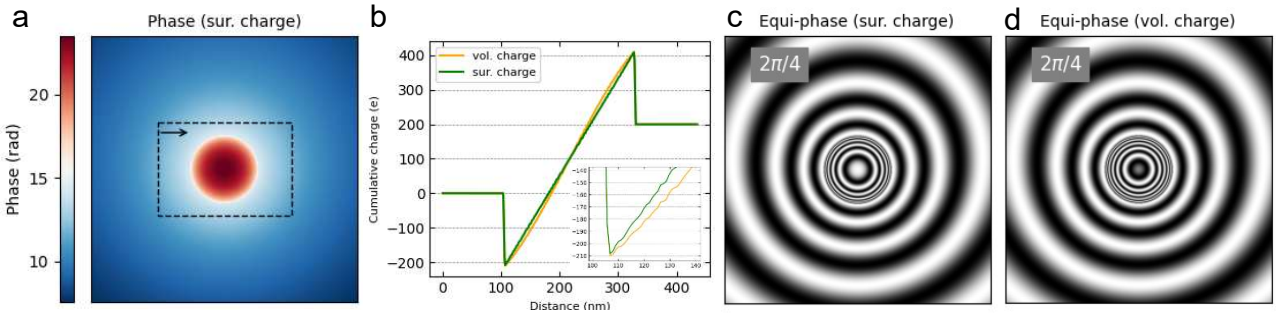


Figure S2: (a) Simulated phase of uniformly surface charged sphere. Charge amount is 200 e, MIP is 5.5 V. The dashed frame is calculation area of cumulative charge using model-independent approach and the arrow is calculation direction. (b) Cumulative charge profiles within the dashed box in (a) of surface charge (green line) and volume charge (orange line) distribution. (c) Equi-phase lines of surface-charged sphere with spacing of $2\pi/4$. (d) Equi-phase lines with spacing of $2\pi/4$ in the case of the uniformly volume-charged sphere.

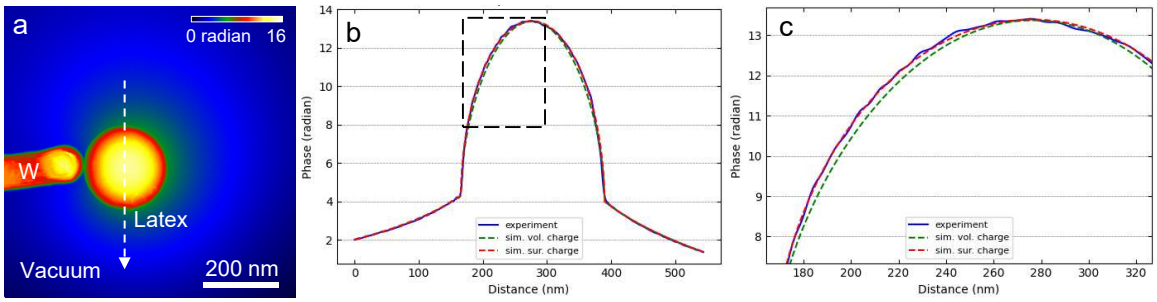


Figure S3: Comparison of phase profile among experiment, surface charge simulation and volume charge simulation.

Figure S3a is the experimental phase image. The dashed arrow is where the phase profile scanning shown in Figure S3b, in which the blue solid line is experiment, red dashed line is surface charge, and green dashed line is volume charge. Both surface and volume charge simulations give charge amount of 140 e , and MIP 5.46 V for surface charge case and 4.85 V for volume case. Both phase profile lines are overlapping in the vacuum part. Within the latex sphere, the phase profile of surface charge model fits the experiment perfectly, but the phase of volume charge model is bit narrow. The enlarge diagram in Figure S3c clearly shows the difference.

# 3 Cumulative charge and MIP

## 3.1 Cumulative charge of surface- and volume-charged sphere

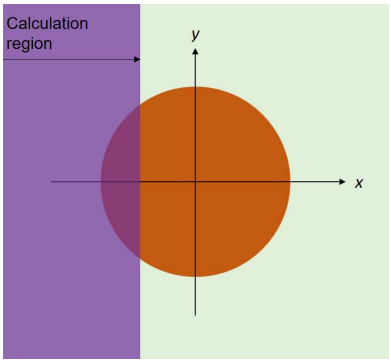


Figure S4: Schematic of charge calculation of a sphere.

Figure S4 shows a schematic of cumulative charge calculation along $x$ axis of a uniformly surface-charged sphere with charge density $\sigma$ and total charge $Q$. By considering that the charge is contained in a spherical cap, whose surface and volume are known analytically [2], it turns out that the cumulative charge amount on the surface $CQ_{\mathrm{S}}$ in calculation region is $CQ_{\mathrm{S}}(x,R) = \sigma S(x,R) = \sigma 2\pi R(R+x) = \frac{Q}{4\pi R^2} 2\pi R(R+x) = \frac{Q(R+x)}{2R}$, where $S(x,R)$ is area of the spherical cap. Considering the full range of $x$, the charge amount can be written as

$$CQ_{\mathrm{S}}(x,R) = \begin{cases} 0 & x < -R, \\ \frac{Q(R+x)}{2R} & -R \leqslant x \leqslant R, \\ Q & x > R. \end{cases} \tag{7}$$

In the case of a constant volume charge density $\rho$ $(= \frac{3Q}{4\pi R^3})$ the cumulative charge amount $CQ_{\mathrm{V}}$ in calculation region is $\frac{1}{3}\pi\rho(2R-x)(R+x)^2 = \frac{Q}{2} + \frac{3Qx}{4R} - \frac{Qx^3}{4R^3}$, so that, considering the

full range of $x$, the charge amount can be written as

$$CQ_{\mathrm{V}}(x,R)=\begin{cases}0 & x<-R,\\ \frac{Q}{2}+\frac{3Qx}{4R}-\frac{Qx^3}{4R^3} & -R\leqslant x\leqslant R,\\ Q & x>R.\end{cases} \tag{8}$$

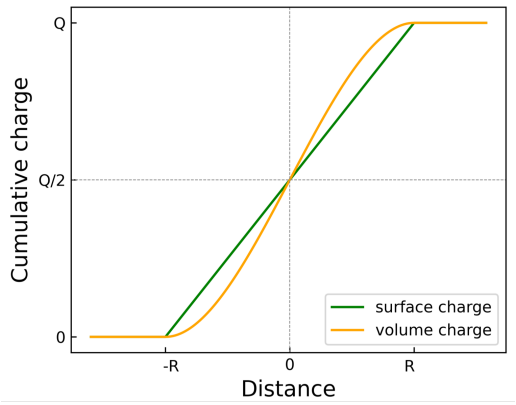


Figure S5: Cumulative charge profiles of a volume charge sphere and surface charge sphere.

The cumulative charge of both cases is reported in Fig. S5, exhibiting a same pattern consistent with that in Ref. [3], which is obtained using a different method.

## 3.2 MIP

The effect of the MIP as regard the integrated charge can be suitably modeled by two concentric spheres of constant surface density and slightly different radii, carrying the same amount of charge so that charge neutrality is assured.

Let us assume that the charge amount on each concentric sphere surface induced by MIP is $Q$, positive for the inner sphere of radius $R$, and negative for the outer one of radius $R+h$, where $h$ is a distance much smaller than $R$. The cumulative charge induced by MIP is therefore given by

$$Q_{\mathrm{MIP}}(x)=CQ_{\mathrm{S}}(x,R)-CQ_{\mathrm{S}}(x,R+h). \tag{9}$$

At the charged boundary $R$, the cumulative charge of these two spheres and total charge are

$$CQ_{\mathrm{S}}(R,R)=Q, \tag{10}$$

$$CQ_{\mathrm{S}}(R,R+h)=\frac{Q(R+h+R)}{2(R+h)}, \tag{11}$$

$$Q_{\mathrm{MIP}}(R)=Q-\frac{Q(2R+h)}{2(R+h)}=\frac{Qh}{2(R+h)}. \tag{12}$$

The cumulative charge of both spheres and the total effect of MIP-induced charge is shown in Fig. S6. In both figures, the cumulative charge increases linearly inside the sphere, further indicating that in the experiments the charge distributes on the surface of latex sphere instead of in the bulk.

Introducing the relationship between $V_{\mathrm{MIP}}$ and $Q_{\mathrm{MIP}}$ as the difference between the potentials of the two spheres, it turns out the following relation with the amplitude of the jump

$$V_{\mathrm{MIP}}=\frac{Q}{4\pi\epsilon_0 R}+\frac{-Q}{4\pi\epsilon_0(R+h)}=\frac{Qh}{2(R+h)}\frac{1}{2\pi\epsilon_0 R}=\frac{Q_{MIP}}{2\pi\epsilon_0 R}. \tag{13}$$

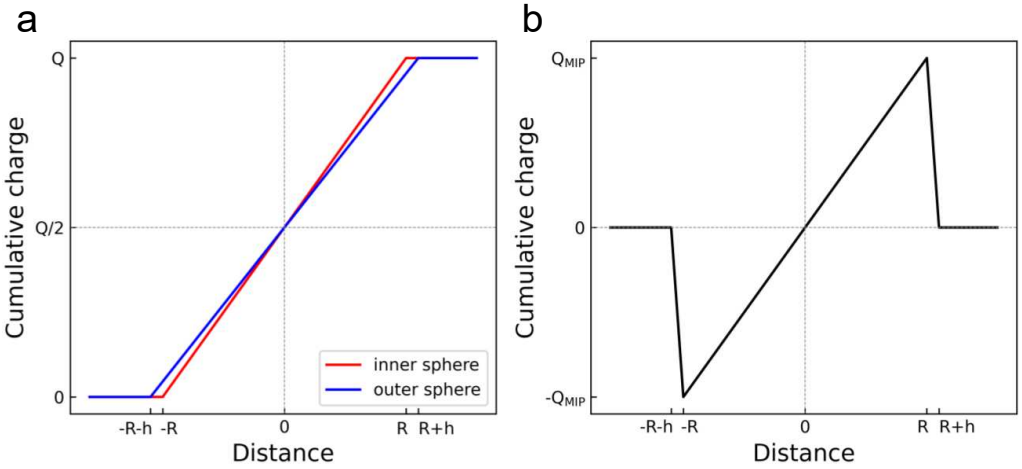


Figure S6: MIP-induced double charge layers and the total effect of MIP on cumulative charge profile.

Therefore, the MIP value can be estimated from the cumulative charge profile. For example in Fig. 1e, $Q_{\mathrm{MIP}}$ is approximately 208 e, substituting into Eq. 13 giving the MIP value of 5.35 V, which is close to the input MIP of 5.5 V.

### 3.3 Cumulative charge in experimental data

Figures S7a and b show the phase images of the latex sphere shown in Fig. 4 in the main text. The dashed boxes frame half sphere. The cumulative charge in vertical and horizontal directions is shown in Fig. S7c and d. The linear profile in both directions indicates that the charge distributes mainly on the surface.

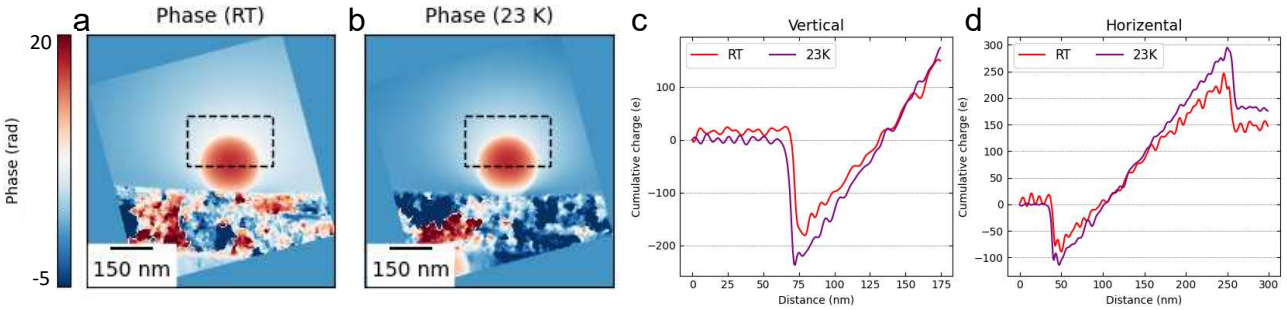


Figure S7: Cumulative charge of the latex sphere shown in Figure 4 in the text. The calculation areas are half of the sphere, indicated by dashed boxes.

Figures S8a to d show the phase images of the latex sphere shown in Fig. 5 in the main text. The dashed boxes frame half sphere. Figures S8e and f present the cumulative charge inside the latex sphere increases linearly. In Fig. S8e, the profile jumps at 70 nm of temperatures 70 K and 5.3 K at result from the phase jumps at the sample boundary due to artifact. Similarly, the profile jumps are also shown in Fig. S8f of temperature 5.3 K.

## 4 Treatment of weighted data

Table S1 displays all data of each latex sphere at different temperatures. A total of 10 latex spheres with different sizes were measured at various temperatures. The uncertainty (or error, $\sigma$) of each value was generated by the different directions surrounding the sphere, as described in the main text and Figs. 1 and 2. The errors of these data are uneven because each measurement

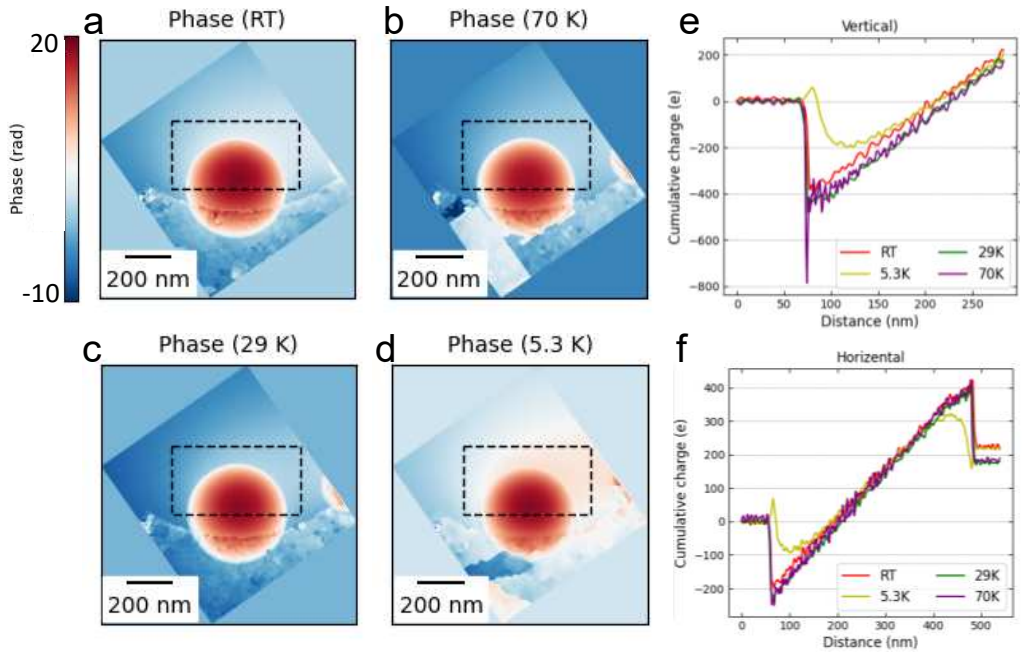


Figure S8: Cumulative charge of the latex sphere shown in Figure 5 in the text. The calculation areas are half of the sphere, indicated by dashed boxes.

has different impacts from sample holders, TEM grids, sample natures, and unpredictable environmental perturbations. Therefore, the data have different precision and the ones with smaller errors have better certainties. Some of the data, like No. 8 at 98 K, the error is actually zero because of the consistency of data. We assign a tiny error to it, $\sigma = 0.01$. Some of the data, for example No. 4 at 5 K and No. 8 at 293 K, were significantly impacted by either the supporting substrate or discontinuous interference fringes, only one effective datum was obtained. We assign a median error value, $\sigma = 0.2$ ($\sigma_{max} = 0.4$, $\sigma_{min} = 0.01$), to these single data.

The larger variance indicates weaker weighting, and the smaller variance referring stronger weighting. The optimal allocation of weights is to make it inversely proportional to the square of its uncertainty. The weighting of $i$th data is $w_i = 1/\sigma_i^2$. Weighted mean by taking the errors into account can be calculated using the formula [4]

$$\bar{x} = \frac{\sum w_i x_i}{\sum w_i}. \tag{14}$$

The weightings of these data are very uneven. If we calculate the weighted standard deviation using $\sigma_{\bar{x}} = 1/\sum w_i^2$, it will result in a fact that the weighted variance is dominated only by the large weightings and degrees of freedom becomes smaller. To correct for this loss of degrees of freedom and get unbiased weighted uncertainties among such uneven weightings, we use the following formula [5]

$$\sigma_{\bar{x}} = \sqrt{\frac{\sum w_i (x_i - \bar{x})^2}{\sum w_i - \frac{\sum w_i^2}{\sum w_i}}}. \tag{15}$$

The weighted mean values and standard deviation are shown in the last raw of Table S1.

Table S1: Diameter, MIP and charge amount of latex spheres at various temperatures from 5 K to 293 K.

| No. | 293 K | 200 K | 150 K | 98 K | 70 K | 29 K | 26 K | 23 K | 5 K | back to RT |
|---|---|---|---|---|---|---|---|---|---|---|
| Sphere 1 | 225.46 ± 2.60 nm<br>5.53±0.04 V<br>145±7 e | | | | | | | | | |
| Sphere 2 | 236.46 ± 0.10<br>5.35±0.21 V<br>200 e | | | | | | | | 228.86±0.89 nm<br>6.07±0.06 V<br>290 e | |
| Sphere 3 | 218.23 ± 1.21 nm<br>5.74±0.19 V<br>280±53 e | | | | | | | 223.22±1.04 nm<br>6.56±0.27 V<br>330±17 e | 217.89±1.67 nm<br>6.25±0.07 V<br>217±47 e | 220.62±1.14 nm<br>5.46±0.24 V<br>217±6 |
| Sphere 4 | 223.90 ± 0.96 nm<br>5.43±0.39 V<br>350±71 e | | | | | | 227.03±1.17 nm<br>6.43±0.18 V<br>335±21 e | | 221.66±2.49 nm<br>5.8±0.2 * V<br>320 e | 221.9±0.53 nm<br>5.68±0.18 V<br>300±28 e |
| Sphere 5 | 213.16±1.22 nm<br>5.7±0.14V<br>220 e | 205.08±1.07 nm<br>6.3±0.14 V<br>150 e | | | | | | | | |
| Sphere 6 | 432.22 ± 1.94 nm<br>5.5±0.14 V<br>470 e | | | | 427.06±2.04 nm<br>6.5±0.21 V<br>370 e | 431.9±2.19 nm<br>6.58±0.18 V<br>420 e | | | 428.02±1.51 nm<br>6.6±0.07 V<br>420 e | 424.87±2.09 nm<br>5.7±0.28 V<br>280 e |
| Sphere 7 | 424.81 ± 1.49 nm<br>5.62±0.2 V<br>500 e | | | | | | | | 425.14±2.44 nm<br>6.5±0.01 V †<br>460 e | |
| Sphere 8 | 430.56 ± 0.95 nm<br>5.7±0.2 V * <br>180 e | | | 427.14±1.7 nm<br>6.2±0.01 V †<br>140 e | | | | | | |
| Sphere 9 | 406.68 ± 2.43 nm<br>5.82±0.16 V<br>480 e | 402.08±1.83 nm<br>6.27±0.06 V<br>700 | 402.98±1.66 nm<br>6.22±0.13V<br>583±29 e | | | | | | | |
| Sphere 10 | 605.99 ± 2.00 nm<br>5.53±0.04 V<br>1333±289 e | | | 602.01±1.66 nm<br>6.03±0.29 V<br>1400±300 e | | | | | | |
| Average MIP | 5.55±0.07 V ‡ | 6.27±0.02 V | 6.22±0.13 V | 6.20±0.12V | 6.50±0.21V | 6.58±0.18V | 6.43±0.18V | 6.56±0.27V | 6.48±0.24 | |

* *These are single data points without errors. A mediate error was manually added for the weighted average and fitting.*
† *These data have no errors due to good concentration. A small error was added for the weighted average and fitting.*
‡ *All RT data both before and after cooling cycle.*

# 5 MIP and diamagnetism

The relationship between MIP and diamagnetic susceptibility $\chi_{dia}$ can be described in the form [6]

$$\chi_{\rm dia} = -\frac{e}{mc^2}V_{\rm MIP} = -1.98\times10^{-6}\cdot V_{\rm MIP}, \tag{16}$$

where $c$ is the speed of light. The diamagnetic susceptibility displays a linear function of MIP. Since the MIP shows a nearly linear function of temperature, the diamagnetism is believed to be proportional to temperature as well.

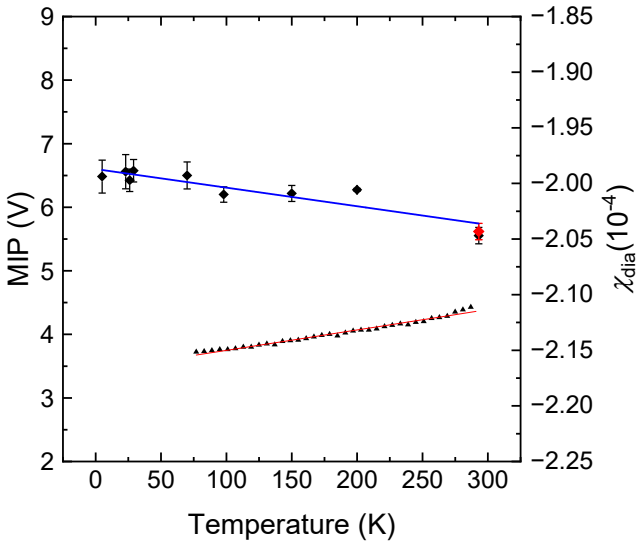


Figure S9: Relationship between MIP and temperature (diamond symbols), and between diamagnetic susceptibility and temperature (triangular symbols).

Superconducting quantum interference device (SQUID), by a Quantum Design MPMS3, was used to measurement the diamagnetism of bulk polystyrene upon temperatures. The diamagnetism is obtained by the form

$$\chi_{\rm dia} = \frac{M}{H}, \tag{17}$$

where $M$ is magnetization (magnetic moment $m$ per unit volume, in unit of A/m) and $H$ is magnetic field intensity (in unit of A/m). All the parameters here are only discussed by their magnitude instead of vector. In the measurement, magnetic moment (in unit of emu) and applied magnetic field B (1 Tesla) are known. B-field and H-field are proportional to each other. Since we are interested in the slope of $\chi_{dia}$ to temperature, therefore, the values of $\chi_{dia}$ shown in Fig. S9 by triangular symbols is actually obtained from the ratio of magnetic moment $m$ (in emu) to B-field, regardless the SI unit. The red line indicates a parabolic fitting in the form

$$\chi_{\rm dia} = (-2.15\pm0.002)\times10^{-4} + (6.88\pm22.31)\times10^{-10}\cdot T + (5.01\pm0.58)\times10^{-11}\cdot T^2. \tag{18}$$

This function is also approximately linear. A fit of the data to a linear function takes the form

$$\chi_{\rm dia} \approx (-2.17\pm0.00054)\times10^{-4} + (1.83\pm0.027)\times10^{-8}\cdot T. \tag{19}$$

According to the relationship between MIP and temperature,

$$V_{\rm MIP} \approx 6.81 - 3.84\times10^{-3}\cdot T, \tag{20}$$

as described in the main text, and Eq. (19), by eliminating $T$, a relationship between the experimental values of MIP and diamagnetic susceptibility over the temperature range between 70 and 300 K is in the form

$$\chi_{\text{dia}} \approx -5.00 \times 10^{-6} \cdot V_{\text{MIP}} - 1.82 \times 10^{-4}. \tag{21}$$

A comparison of the coefficient in $V_{MIP}$ in Eq. (16) of $-1.98 \times 10^{-6}$ with that in Eq. (21) of $-5.00 \times 10^{-6}$ reveals a discrepancy of a factor of 2.5, the fact that the two values are on the same order demonstrates reasonable consistency between the experimental and theoretical results in the temperature range from 70 K to 300 K. On the other hand, the values of $\chi_{dia}$ from 0 to 70 K, which are absent in the figure, increase significantly as temperature decreases.

# References


[1] J.D. Jackson and R.F. Fox. Classical electrodynamics, 1999.

[2] A.D. Polyanin and A.V. Manzhirov. *Handbook of mathematics for engineers and scientists*. Chapman and Hall/CRC, 2006.

[3] M. Beleggia, L.C. Gontard, and R.E. Dunin-Borkowski. Local charge measurement using off-axis electron holography. *Journal of Physics D: Applied Physics*, 49(29):294003, 2016.

[4] P.R. Bevington and D.K. Robinson. Data reduction and error analysis. *McGrawâ€“Hill, New York*, 2003.

[5] J. Kirchner. Data analysis toolkit# 12: Weighted averages and their uncertainties. *University of California: Berkeley, CA*, 2006.

[6] J.E. Hirsch. Superconductivity, diamagnetism, and the mean inner potential of solids. *Annalen der Physik*, 526(1-2):63–78, 2014.